Springer

KSME

Journal of Mechanical Science and Technology 24 (5) (2010) 1151~1162
www.springerlink.com/content/1738-494x
DOI 10.1007/s12206-010-0321-8

Optimum design of 6-DOF parallel manipulator with translational/rotational workspaces for haptic device application †

Jung Won Yoon[1,*], Jeha Ryu[2] and Yoon-Kwon Hwang[1]

[1]*School of Mechanical and Aerospace Engineering and ReCAPT, Gyeongsang National University, Jinju, Korea*
[2]*Human-Machine-Computer Interface, Department of Mechatronics, Gwangju Institute of Science and Technology, Gwangju, Korea*

(Manuscript Received June 9, 2009; Revised February 2, 2010; Accepted February 26, 2010)

Abstract

This paper proposes an optimum design method that satisfies the desired orientation workspace at the boundary of the translation workspace while maximizing the mechanism isotropy for parallel manipulators. A simple genetic algorithm is used to obtain the optimal linkage parameters of a six-degree-of-freedom parallel manipulator that can be used as a haptic device. The objective function is composed of a desired spherical shape translation workspace and a desired orientation workspace located on the boundaries of the desired translation workspace, along with a global conditioning index based on a homogeneous Jacobian matrix. The objective function was optimized to satisfy the desired orientation workspace at the boundary positions as translated from a neutral position of the increased-entropy mechanism. An optimization result with desired translation and orientation workspaces for a haptic device was obtained to show the effectiveness of the suggested scheme, and the kinematic performances of the proposed model were compared with those of a pre-existing base model.

Keywords: Parallel manipulator; Optimization; Genetic algorithm; Haptic device; Translation and orientation workspaces; Isotropy

1. Introduction

Parallel manipulators offer several advantages over serial manipulators: higher stiffness, smaller link masses, large payloads, and higher accuracy. These advantages have prompted the development of many parallel manipulators with different mechanism configurations [1-3]. Some drawbacks also exist: a small workspace, different kinematic characteristics for each axis, singularities inside the workspace, and others. For these reasons, many researchers have attempted to discover new techniques that can increase the size of the workspace while maximizing the isotropy of the mechanism and avoiding the internal singularities [4-7]. Tsai and Huang proposed a method for designing an isotropic six-DOF parallel manipulator developed from an isotropy generator, consisting of six straight lines satisfying the isotropy conditions [8]. They used the device to develop an isotropic Stewart–Gough parallel manipulator. Tsai and Zhou proposed isotropic parallel designs with an optimum global isotropy using an isotropy generator [9]. Gallant and Boudreau presented an optimization scheme for planar parallel manipulators with prismatic joints to obtain a workspace as close as possible to the prescribed workspace and maximize their global dexterity [10]. As a result, singularity-free workspaces in which the singularity loci are located outside of the workspace could be created. Monsarrat and Gosselin proposed an optimization procedure to maximize the volume of a constant-orientation workspace of a parallel manipulator [11]. Moreover, they developed another volume maximization scheme with a new workspace having coupled translational and rotational DOFs (z, and the tilt and azimuth angles) in a cylindrical system for a motion base application in flight simulators. Yoon and Ryu developed a new general-purpose six-DOF haptic device with parallel manipulators, which has a good set of kinematic characteristics such a small moving inertia owing to the base-fixed actuators, a large orientation workspace with a RRR spherical joint, no singularities inside the workspace, and relatively simple forward kinematics [12].

The size of the workspace and the isotropy are important indices of the kinematic performance of parallel manipulators. Most research to date has evaluated the performance indices of the mechanism at a neutral posture in which the translation and orientation workspaces of the end-effector were calculated. However, a mechanism with a large orientation workspace (OW) at a neutral posture may not have a proportionally large OW throughout the three-dimensional (3-D) translation work-

† This paper was recommended for publication in revised form by Associate Editor Doo Yong Lee

*Corresponding author. Tel.: +82 55 751 6078, Fax.: +82 55 752 0227
E-mail address: jwyoon@gnu.ac.kr

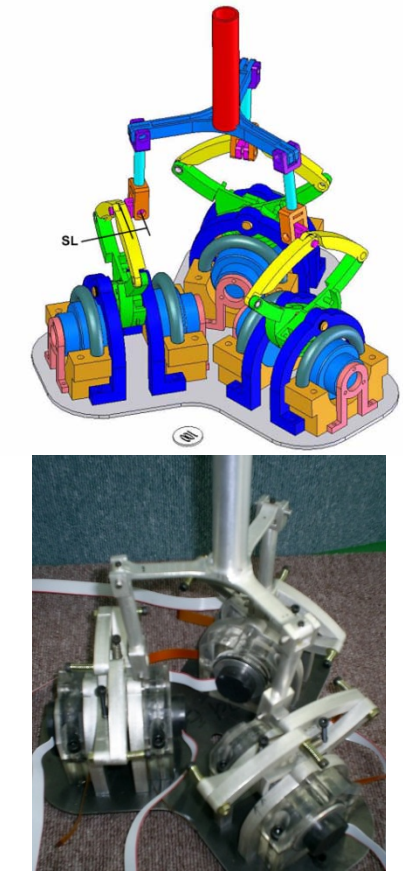

Fig. 1. Proposed six-DOF haptic device.

spaces, due to the complicated multi-linkage mechanism structures of parallel manipulators. The orientation workspace of most 6-dof parallel manipulators usually decreases rapidly in size as the distance from the neutral position increases [12]. Thus, it is difficult to apply this parallel manipulators type to a haptic device that requires simultaneously large 3-D translational and rotational motions over the entire workspace. Most six-DOF parallel manipulators for applications with both positioning and orienting motions have these types of difficulties, and cannot guarantee good amount of rotational motion throughout the prescribed 3-D translation workspace [13].

In this paper, we propose an optimum design method for parallel manipulators that can guarantee the required orientation workspace throughout the prescribed 3-D translation workspace while maximizing the isotropy of the system. The proposed method discretizes a prescribed bounding 3-D translation workspace that can be described approximately by a sphere, and then discretizes an orientation workspace represented in a cylindrical system at each boundary point of the discretized prescribed translation workspace. An objective function is calculated in the optimization process using a genetic algorithm to satisfy desired translation and orientation workspaces and maximize the global conditioning index (GCI). An optimum design result for a haptic device was obtained to show the effectiveness of the suggested scheme: it

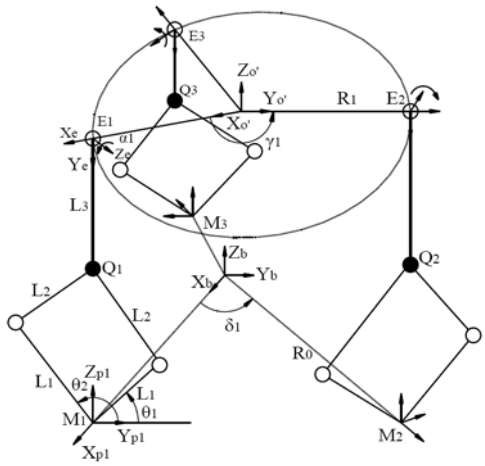

Fig. 2. Kinematic model.

was compared with a base model of half the size of the pre-existing base model described in [12].

The organization of this paper is as follows. The kinematic descriptions and design requirements of the proposed six-DOF parallel manipulator are given in Sections 2 and 3, respectively. In Section 4, the optimization problem is formulated using a simple genetic algorithm. Optimum design results and kinematic performance comparisons with the base model are presented in Section 5, and our conclusions and future work are summarized in Section 6.

2. Kinematic description of six-DOF parallel manipulator

The proposed six-DOF haptic device, shown in Fig. 1, is similar to the parallel mechanism given in [12] in terms of having three pantograph mechanisms that are driven by six base-fixed servomotors with three RRR spherical joints at the top of the pantograph mechanism, an end-effector, and connecting bars. This device provides a good load capacity and wide orientation workspace, with no singularities inside the workspace.

The kinematic parameters used to obtain the static characteristics of the mechanism are shown in Fig. 2. The global reference frame, denoted by Σ_b (X_b, Y_b, Z_b), is located at the center of the base plate. The local frames of the end-effector and each pantograph are denoted by $\Sigma_{o'}$ ($X_{o'}$, $Y_{o'}$, $Z_{o'}$) and Σ_{pi} (X_{pi}, Y_{pi}, Z_{pi}), respectively where i = (1, 2, 3). The axisymmetric positions of each pantograph and revolute joint are given by the angles δ_i and γ_i (I = 0, 2/3 π, 4/3 π) with radii of R_0 and R_1. Each pantograph has two-DOF motion in the Y_{pi}–Z_{pi} plane. Even though the spherical joints appear to be located at the top of the pantograph mechanisms, the actual centers are located at an offset distance of *SL* (see Fig. 1). In the kinematic analysis, however, the center of the spherical joint was assumed simply to be on top of the pantograph mechanism, because the offset distance does not affect the results if R_0 is replaced by $R_0 - SL$. The upper and lower links of the pantograph and the

connecting bar are denoted by L_1, L_2, and L_3, and the positions of the active, spherical, and revolute joints are given by M_i, Q_i, and E_i, respectively.

In the inverse kinematics calculations, the active joint angles θ_{1i} and θ_{2i} of each pantograph are obtained for a given position and rotation (x, y, z, φ, θ, γ) of the end-effector. The Jacobian matrix can be easily derived using the concept of reciprocal screws. The mechanism singularity occurs when the pantograph mechanisms are either lowered down to the base plate plane or are raised vertically, or when all of the connecting bars are perpendicular to the pantograph planes. These configurations are outside of the mechanism workspace. More details are given in reference [12].

3. Design requirements

Optimum design of compact haptic devices that can be used in complicated and sophisticated applications entails some static mechanical requirements: a small size for the low inertia requirement in haptic applications, a large workspace for dexterous manipulation, and good isotropy for homogeneous kinematic quality over the entire workspace. This section describes the linkage parameters and design variables, the desired discrete translational and orientation workspaces, and the global conditioning index (GCI), which are used to specify those requirements.

3.1 Linkage parameters and design variables

The linkage parameters determining the size of the haptic device are L_1, L_2, L_3, R_0, R_1, and SL (see Figs. 1 and 2). The RRR-type spherical joint, however, does not permit full rotation, due to the link interference between the connecting link L_3 and the offset SL, even though it has a large rotation range. Therefore, the existing device [12] was developed using SL as a design variable to maximize the rotation angle of L_3 for a large workspace. The parameters of the base model with which the proposed optimized models are compared are chosen as half of the parameter values in the existing model shown in Table 1 for a more compact size and the same orientation workspace as the base model. The lower and upper link lengths (L_1 and L_2) of the pantograph mechanism are set to the same values for simplicity of design. Also, the base radius (R_0) and mobile radius (R_1) are set for the relationship $R_1 = R_0 - SL$ to increase the isotropy of the mechanism [12]. As a result, only the three variables L_1, L_3, and R_0 are used as design variables to calculate the objective function by the genetic algorithm in the optimization process.

In the following optimization process, we define a neutral position as the position of the end-effector center point when the actuators are actuated at the middle of the full motion ranges. For example, $\theta_{1i} = 30^\circ$ and $\theta_{2i} = 150^\circ$ are the middle motions for rotary motions in Fig. 3. Note that the neutral position **P** (0, 0, P_z) of the end-effector along the Z axis in Σ_b can be considered a factor for evaluating the compactness of the haptic device when the base and the mobile radii are fixed. In fact, P_z in Table 1 can be computed as

Table 1. Linkage parameters of existing model [12].

Values of linkage parameters						
P_z	L_1	L_2	L_3	R_0	R_1	SL
240 mm	80 mm	80 mm	160 mm	130 mm	100 mm	30 mm

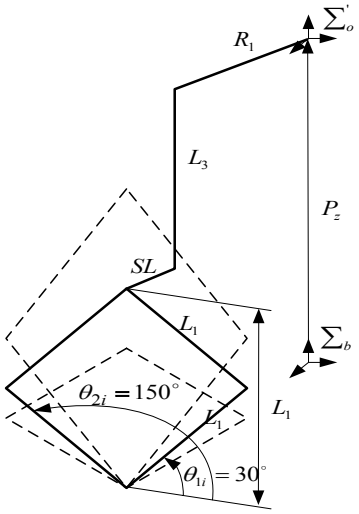

Fig. 3. Neutral position P_z of end-effector when θ_{1i} = 30° and θ_{2i} = 150°.

$$P_z = \sin(\theta_{1i})L_1 + \sin(\theta_{2i})L_2 + L_3 \quad (i=1, 2, 3) \tag{1}$$

where $0^\circ \le \theta_{1i} \le 90^\circ$ and $90^\circ \le \theta_{2i} \le 180^\circ$, and $L_3 \le P_z \le L_1 + L_2 + L_3$.

3.2 Desired discrete translation workspace

For simplicity of optimum design, a desired translation workspace (TW), denoted by Ω_r, can be specified by a sphere whose center is located at **P** (0, 0, P_z) in Σ_b, where the subscript r represents the desired radius of the sphere. A spherical shape is selected because the shape of the real translation workspace of the suggested mechanism in Fig. 1 is roughly spherical, rather than cubical as in [12]. If another shape is desired, the same design philosophy as will be explained in this paper can be used. To implement the genetic algorithm, the desired 3-D translation workspace in which the isotropy of the mechanism is evaluated is bounded and discretized as shown in Fig. 4. It should be noted that the center of the sphere that is at the neutral position **P** (0, 0, P_z) in Σ_b can also be determined according to the change of the design parameters (i.e.; $P_z = L_1 + L_3$) during the optimization process. Since the moving ranges of actuators become the largest at the neutral position, the end-effector of the suggested mechanism has wider translation and orientation motion ranges at the neutral position than at the boundary position. Therefore, if a real workspace of the suggested mechanism includes the boundary surface of a desired translation workspace, it can also include

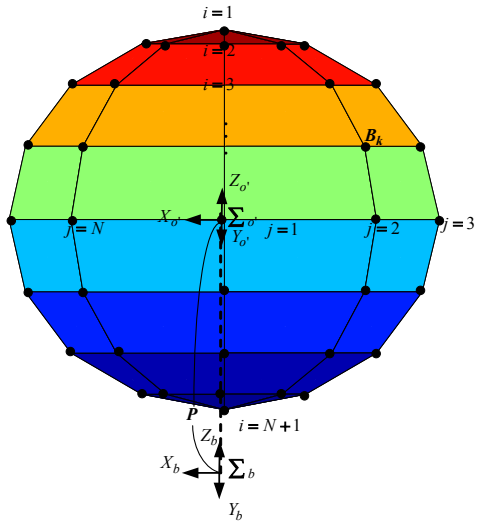

Fig. 4. Discretization positions $\mathbf{B}_k$ of spherical surface for translation workspace Ω_r.

all positions inside the boundary surface. Only the outer surface of a sphere rather than the inside of a spherical volume, therefore, is discretized for the orientation workspace evaluation. This limited discretization can effectively reduce the computation load of the optimization process.

Ω_r can be discretized to discrete translation points $\mathbf{B}_k(X_k, Y_k, Z_k)$, where k =1, 2, 3, ⋯, N *(N-1)*+2, as shown in Fig. 4. The number of discretized horizontal points of Ω_r is N+*1* (i = 1, 2, 3, ⋯, N+*1*), while the number of discretized vertical points is N (j = 1, 2, 3, ⋯, N). Thus, the total discretized number N_{tot} =N *(N-1)*+2. For each discretized point, the inverse kinematics problem is solved and the solution is checked against mechanical constraints such as design variable constraints and range of motions of spherical joint pairs. If the solution is inside the limits of the design variables and does not violate the mechanical constraints, the discretized point belongs to Ω_r. This means that the discretized point is inside the real translation workspace. If all points of $\mathbf{B}_k$ are located inside the real workspace during the optimization process, the condition for a desired translation workspace of spherical shape will be satisfied.

3.3 Desired discrete orientation workspace

The desired orientation workspace (OW) can be specified using the projected OW, which is based on the use of a modified set of Euler angles and a particular representation of the rotational workspace in a cylindrical coordinate system [14]. The projected OW was defined as the set of possible directions for the approach vector of the end-effector and the intersection of the rotational workspace volume with a plane of zero roll angle, as shown in Fig. 5. The projected OW for the desired orientation workspace is selected because it shows intuitively a tilt angle θ between the tool approach vector and the base z-axis at the azimuth angle φ, and it is computationally simple with ψ=0°.

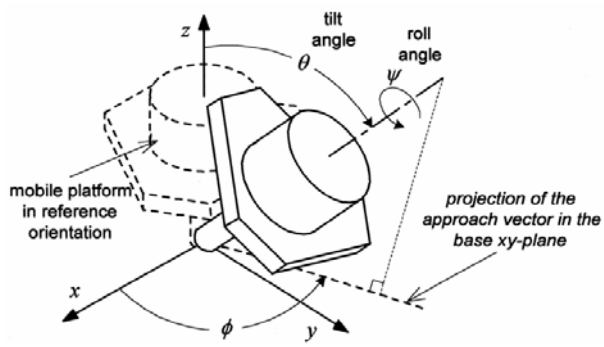

Fig. 5. Modified Euler angles [14].

Thus, the desired orientation workspace can be specified by the projected OW $\Gamma(\theta_{\min})$ at the boundary surface of a desired translation workspace, where the subscript $\theta_{\min}$ represents the desired minimum tilt angle. Note that the origins of the projected OW are located on the spherical surface of the desired translation workspace. If the suggested mechanism satisfies the desired orientation workspace at the boundary surface of a desired translation workspace, the mechanism can also satisfy the desired orientation workspace inside the desired translation workspace.

The desired discrete orientation workspace $\Gamma_{l,k}(\theta_{\min})$ for the projected OW can be discretized with respect to the discrete azimuth angle φ_l at each discrete point $\mathbf{B}_k(X_k, Y_k, Z_k)$ of the boundary surface of the desired translation workspace (see Fig. 6), where l= 1, 2, 3, ⋯, M+1, within a 0° - 360° range of φ. The total number M_{tot} of discretized angles for $\Gamma_{l,k}(\theta_{\min})$ is therefore (M + 1) N_{tot}, where N_{tot} is a total discretized number of $\mathbf{B}_k$, as explained in Section 3.2. Similarly to the case for the translation workspace, the condition for the desired orientation workspace can be satisfied by solving the inverse kinematics problem. That is, if all of the tilt angles of $\Gamma_{l,k}(\theta_{\min})$ at the boundary surface of the desired translation workspace are larger than $\theta_{\min}$ during the optimization process, a real projected OW will have larger tilt angles than $\theta_{\min}$ throughout the desired translation workspace.

3.4 Global conditioning index with homogenous jacobian matrix

The global conditioning index (GCI) is typically used to represent the isotropy of a parallel mechanism. It was introduced by Gosselin and Angeles [15], and represents one of the performance indices in the manipulator optimal design process that involves a distribution of the condition number over the workspace. The condition number is defined as

$$c = \frac{\sigma_{\max}}{\sigma_{\min}} \tag{2}$$

where $\sigma_{\max}$ and $\sigma_{\min}$ represent the maximum and minimum singular values of the manipulator Jacobian **J**. Since the condition number c can range from 1 to ∞, the index $\eta = 1/c$ is used

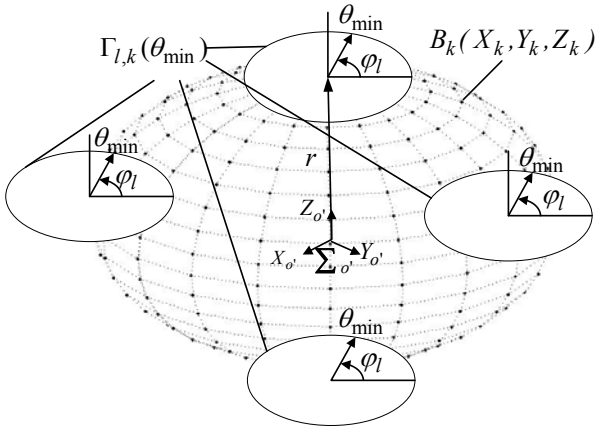

Fig. 6. Desired discrete orientation workspace $\Gamma_{l,k}(\theta_{\min})$ at each discrete translation points $\mathbf{B}_k$ (X_k, Y_k, Z_k).

to bound the index between 0 and 1, where a value of unity represents a perfectly isotropic matrix.

However, several researchers have argued that, due to the dimensional non-homogeneity of **J**, the condition number may not have any physical or geometrical meaning for a 6-DOF manipulator with both translational and rotational motions. The use of the characteristic length [16] and the homogeneous Jacobain formulation [17] by three end-effector points were suggested as a solution to non-homogenous Jacobian matrix problems. Recently, Nawratil proved that the characteristic length should not be the result of an optimization procedure but rather a design constant, which must be predefined. He suggested that a geometric interpretation of the characteristic length CL can be explained as $CL=R\sqrt{\frac{2}{3}}$, where R is the radius of the operation sphere that is a part of the end-effector [18]. Thus, in this paper, the homogenous Jacobian $\mathbf{J_H}$, is defined as

$$J_H = JL\,,\quad L=\begin{bmatrix} I_3 & O_3 \\ O_3 & \dfrac{I_3}{CL} \end{bmatrix} \tag{3}$$

where the 3×3 identity matrix $\mathbf{I}_3$ and the 3×3 zero matrix $\mathbf{O}_3$ can form the homogenous Jacobain matrices by use of the characteristic length.

After η is obtained at the position $\mathbf{B}_k$ for the homogenous Jacobian $\mathbf{J_H}$, GCI is computed over the discrete translation workspace as

$$\text{GCI}=\frac{\int_w \eta dw}{\int_w dw},\quad 0 \le GCI \le 1 \tag{4}$$

where w represents the discrete translation workspace described in Section 3.2. Note that GCI close to unity provides a more even feel throughout the translation workspace of a haptic device.

4. Formulation of optimization problem

4.1 Application of genetic algorithm

Most real-world optimization problems are difficult to solve because not only are they complicated but also there is no sufficient information about the reciprocal relationship between design variables and *a priori* knowledge of the optimization problems. The genetic algorithm is a probability-based optimization method that describes genetics and natural evolution numerically [19, 20]. The method is based on the creation and evolution of many individuals that become stronger through several generations. For the optimal mechanism design process, each randomly created individual represents a set of mechanism parameters. The strength of these individuals (L_1, L_3, R_0) is evaluated using an objective function that is set up for the optimization goals of the mechanism. The evolution of the individuals is accomplished using genetic operators, such as selection, crossover, and mutation, until the method converges toward an optimal solution. The method is especially useful for the proposed model, which has a complicated mechanism. Also, it robustly searches for a globally optimized solution [21].

4.2 Objective function

An objective function $F(x)$ can be computed from the synthesis of individuals using the genetic algorithm

$$F(x) = MAX\{\varpi_1 \frac{n_{in}}{N_{tot}} + \varpi_2 \sum_{i=1}^{n_{in}} \frac{M_{i,in}}{M_{tot}} + \varpi_3 GCI\} \tag{5}$$

where n_{in} and $M_{i,\,in}$ are the number of discretized points and angles that fall in the desired translation workspace Ω_r and the desired projected OW $\Gamma(\theta_{\min})$ with respect to discrete point $\mathbf{B}_i(X_i, Y_i, Z_i)$, respectively, and $\varpi_1, \varpi_2, \varpi_3$ are the weighting factors for each term. It should be noted that N_{tot} and M_{tot} are the total number of discretized points and angles and that the desired projected OW and the GCI will be computed only at the discretized points (i=1, 2, ⋯, n_{in}) of the spherical surface that are included in the desired translation workspace. The first term in Eq (5) is chosen to satisfy the desired translation workspace with a given radius r of the sphere as well as to make the translation workspace (TW) as close as possible to a spherical shape. If n_{in} equals N_{tot}, then the real TW includes the desired spherical shape. The second term is selected to satisfy the desired minimum tilt angle $\theta_{\min}$ with respect to the azimuth angle φ at each boundary point of the desired translation workspace. If $\sum_{i=1}^{n_{in}} M_{i,in}$ equals M_{tot}, then the real projected OW satisfies the desired OW condition. The third term GCI is employed to maximize the isotropy over the translation workspace as well as to avoid singularities inside the workspace. With $\varpi_1 = 1, \varpi_2 = 1, \varpi_3 = 1$, all terms in Eq. (5) will have equal contributions to the objective function. The suggested multi-objective function will then satisfy the desired

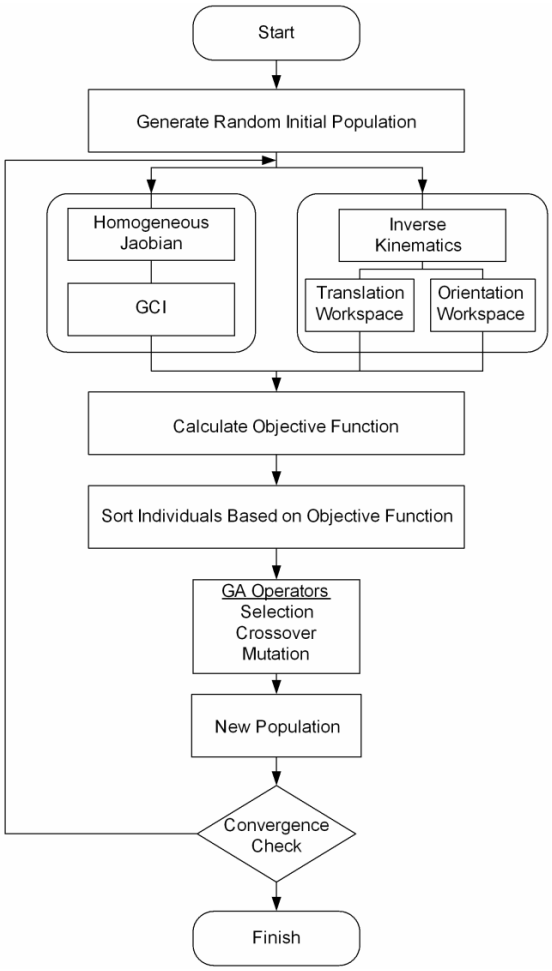

Fig. 7. Flowchart of optimization process.

orientation workspace at the boundary surface of the desired translation workspace, and will maximize the isotropy inside the translation workspace through the optimization process, as shown in Fig. 7. Through the optimization, the desired translation workspace Ω_r with the prescribed sphere of radius r will be located inside a real translation workspace and the desired orientation workspace will make a real projected OW include the prescribed tilt angle θ_{min} throughout the desired translation workspace; also, the shapes of two workspaces will become more regular by increasing the GCI.

4.3 Constraints on design variables

The objective function in Eq. (5) is computed only within the design variable constraints that can be obtained by analyzing the expected motion in advance. To ensure that we obtain the optimal solution for Eq. (5) in the imposed solution space, not only the range of the linkage lengths but also the initial posture and the singularity configuration of the mechanism must be considered. Since the parameters L_1, L_3, and R_0 are selected as design variables, all of the other parameters are selected as constraints: $L_2 = L_1$, $SL = 15$, $R_1 = R_0 - SL$, and P_z by L_1 and L_3 at $\theta_{1i} = 30°$ and $\theta_{2i} = 150°$. Accordingly, the design variable constraints for the system boundary are

$$\Lambda = \{x \mid x^{(L)} \le x \le x^{(U)}\} \tag{6}$$

where $\boldsymbol{x}^{(L)}$ is the lower limiting vector and $\boldsymbol{x}^{(U)}$ is the upper limiting vector for $\boldsymbol{x} = (L_1, L_3, R_0)$. Each limiting vector range is shown in Table 2. We set $\boldsymbol{x}_{init}$ to the base model value vector, and set $\boldsymbol{x}^{(L)}$ and $\boldsymbol{x}^{(U)}$ to $\pm 60\%$ of the base model value vectors. If the desired translation and orientation workspaces and the GCI are not satisfied through the optimization process, then $\boldsymbol{x}^{(U)}$ can be extended as

$$x^{(U)} = x_{init}(1 + W_b) \tag{7}$$

where W_b is the constraint range gain. Thus, W_b is initially set to 0.6.

In order to avoid singularities in the workspace, analytical singularity equations can be utilized as nonlinear constraints as in [11]. However, these singularity constraints are not considered in the proposed mechanism design since the mechanism has no singularities inside the workspace. Note that the GCI can also be used to prevent the mechanism from being close to singular configurations.

Table 2. Range of constraints with W_b=0.6.

Variables								
L_1			L_3			R_0		
x_{init}	$x^{(U)}$	$x^{(L)}$	x_{init}	$x^{(U)}$	$x^{(L)}$	x_{init}	$x^{(U)}$	$x^{(L)}$
40 mm	64 mm	16 mm	80 mm	128 mm	32 mm	65 mm	104 mm	26 mm

x_1	x_2	x_3
48	96	78
⬇		
s_1	s_2	s_3
110000	1100000	1001110
⬇		
l_1	l_2	l_3
6	7	7

Fig. 8. Binary encoding of $\boldsymbol{s}$ and chromosome length $\boldsymbol{l}$ for real vector $\boldsymbol{x}$.

4.4. Encoding of parameters

The genetic operators and the robustness are performed in two spaces of coding based on the binary string and the solution, which is based on parameters. To represent points in the search space, each range of feasible region for the constraints is transformed to a natural parameter, called a string or chromosome, in the coding space, as shown in Table 2. Fig. 8 shows the procedure that transforms constraint $\boldsymbol{x}$ from the vector of binary string $\boldsymbol{s}$ into the vector of chromosome length $\boldsymbol{l}$. The constraint x_i is obtained from the range of feasible re-

gion Λ in Eq. (6), the binary string s_i is calculated through the binary encoding of x_i, and subsequently, the chromosome length l_i is obtained with the following equation:

$$l_i \geq \log_2 [\ (|x_i^{(U)}|-|x_i^{(L)}|)10^{d_i}+1] \ (i = 1\sim3) \tag{8}$$

where the resolution of the digit for each parameter is d_i = (0,0,0). From Eq. (8), the total length of chromosome l becomes 20-bits.

The initial population has to be generated in order to perform the simulated evolution through the genetic operators. The population takes on he role of integral memory while evolving individuals. The population, denoted by P_a (k), in the k-th generation is defined as a set of individuals for the number of N:

$$P_a(k) = [s_1(k), s_2(k), \ldots, s_{NP}(k)], \tag{9}$$

where s_i (k) is a point in search-space as the i-th chromosome and N_P (>1) is the population size. The initial population P_a (0) is generated by the random initialization method. This method initializes the chromosome as a binary constant, of which the number of Nl is generated by the random number generator. If the number of individuals in a population (N_P), Maximum number generations, Probability of crossover (P_c), and Probability of mutation (P_m) are 100, 50, 0.85, and 0.05, respectively, the total bit number becomes 100*20 = 2000. In addition, the number of chromosomes generated by crossover is P_cN_P = 0.85*100 = 85, and the number of bits generated by the mutation at each generation is P_mN_Pl = 0.05*100*20 = 100.

5. Optimum design results

5.1 Optimum results with suggested scheme

In this section, optimum design results are obtained using the suggested optimization process. For optimization, the radius r of a sphere for a desired translation workspace and the minimum tilt angle $\theta_{\min}$ for a desired orientation workspace should be initially determined. For the translation workspace, we aim to design a compact haptic device like PHANTOM® Omni ™, a commercialized haptic device of compact size, the success of which has been proven by its high demand in the market as a device that complies with design standards determining suitability for optimization. However, if the desired radius for a desired TW is set over 30mm, the size of the designed mechanism become larger than the PHANTOM® Omni™ in height (about 200mm). Thus, the desired radius r is set to 30mm and the desired minimum tilt angle $\theta_{\min}$ is set to 45°, as a haptic device might need a large OW while satisfying TW. It should be noted that the maximum tilt angle of the base model was about 45° at the neutral position [12].

For discretization of the workspaces, N and M are set to 10 and 361, respectively. These values result in 92 discrete points for the desired TW and a step angle of 1° for the desired OW. Table 3 shows the parameters used for the genetic algorithm.

Table 3. Parameters used for genetic algorithm.

Parameters	
Number of individuals in population	50
Maximum number of generations	300
Probability of crossover	0.80
Probability of mutation	0.01

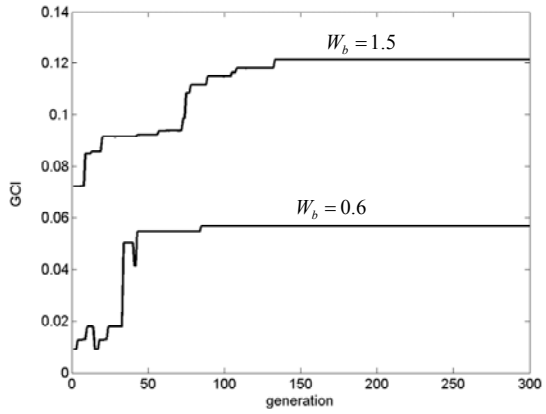

Fig. 9. GCI with respect to upper ranges of design variables.

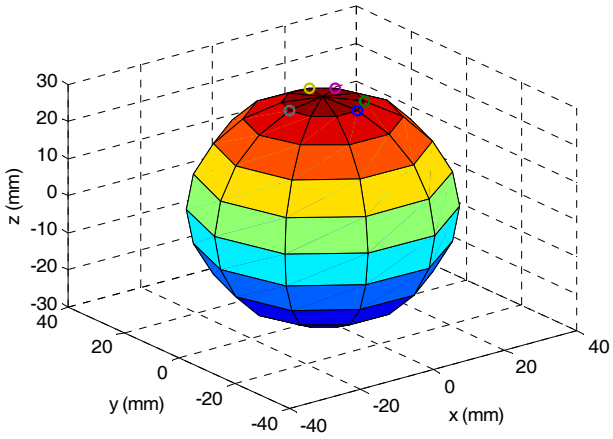

Fig. 10. Weakest points of orientation among boundary positions in Σ_o by optimization with N=10, Ω_{30}, and $\theta_{\min} = 45^\circ$.

Based on the desired workspaces, the L_1, L_3, and R_0 parameter values with P_z were obtained through the suggested optimization scheme. Since the optimized parameters had a lower GCI than that of the base model with W_b=0.6 in Eq. (7), the upper ranges of the design variables were extended so as to have a larger GCI, by increasing the gain W_b to 1.5, as shown in Fig. (9).

Real projected OWs are given at the weakest point of orientation on the boundary positions of Ω_r to show that a real projected OW can satisfy a desired minimum tilt angle even in the worst case. The weakest point on the boundary surface of Ω_r can be defined as the point that has the smallest minimum tilt angle of the real projected OW. Fig. 10 shows the weakest points of orientation among the boundary positions in Σ_o after optimization with N=10, Ω_{30}, $\theta_{\min} = 45^\circ$, and

Table 4. Performance trends with respect to parameters.

Index \ Parameter	R_0	L_1=L_2	L_3
OW↑	↓	↑	↓
TW↑	*const*	↑	↑
GCI↑	↑	↓	↓
P_z↑	*const*	↑	↑

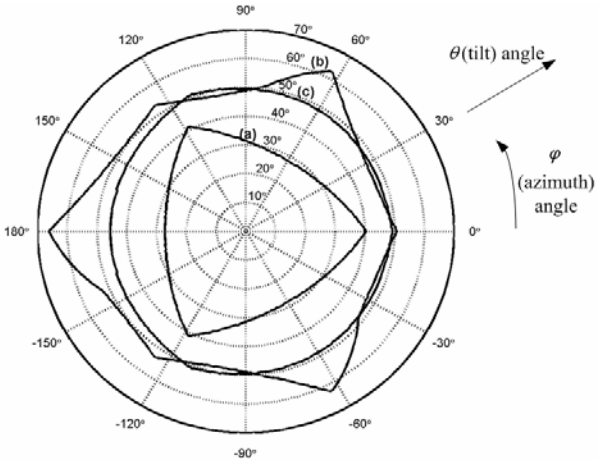

Fig. 11. Projected OWs at each boundary position **B** (-9.3, 0, 28.5) in $\Sigma_{o'}$ with Ω_{30} and $\theta_{\min} = 45^\circ$: (a) $\varpi_1 = 1, \varpi_2 = 0, \varpi_3 = 1$ (b) $\varpi_1 = 1, \varpi_2 = 1, \varpi_3 = 0$ (c) $\varpi_1 = 1, \varpi_2 = 1, \varpi_3 = 1$.

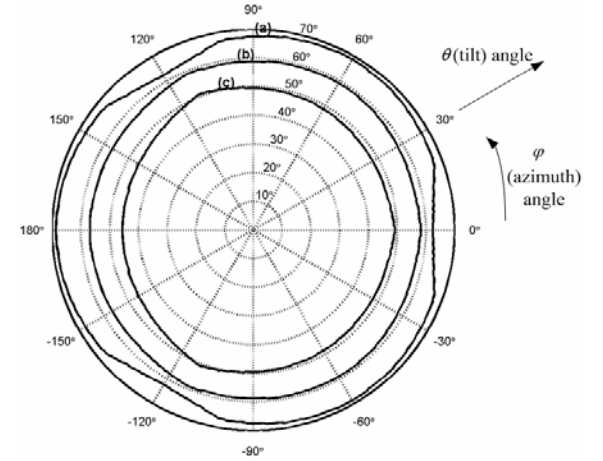

Fig. 12. Projected OWs at different locations inside desired TW with $\theta_{\min} = 45^\circ$ & Ω_{30} : (a) neutral position **B** (0, 0, 0) of Ω_{30} in $\Sigma_{o'}$ (b) inside position **B** (-4.6, 0, 14.3) of Ω_{30} in $\Sigma_{o'}$ (c) boundary position **B** (-9.3, 0, 28.5) of Ω_{30} in $\Sigma_{o'}$.

$\varpi_1 = 1, w_2 = 1, \varpi_3 = 1$. It should be noted that the weakest point is not unique, but is located around the top of the sphere surface. This phenomenon can occur, because the upper part of the real TW is closer to a spherical shape than the lower part of the real TW, which will be shown in Section 5.2.

In order to demonstrate the role of each term in Eq (5), three cases of optimization are studied: (a) the optimization of GCI with respect to a desired TW ($\varpi_1 = 1, w_2 = 0, \varpi_3 = 1$), (b) the optimization of a desired OW with respect to a desired TW without the optimization of GCI ($\varpi_1 = 1, w_2 = 1, \varpi_3 = 0$), (c) the optimization of a desired OW and GCI with respect to a desired TW ($\varpi_1 = 1, w_2 = 1, \varpi_3 = 1$). For each case, Fig. 11 shows the projected orientation workspace (OW) of the end-effector at the boundary point **B** (-9.3, 0, 28.5) in the $\Sigma_{o'}$ of Ω_{30}, which is one of the weakest points. Fig. 11(a) shows that the minimum tilt angle of the projected OW at the boundary position of Ω_{30} in the case of (a) ($\varpi_1 = 1, w_2 = 0, \varpi_3 = 1$) is below 27°, which says that the desired orientation workspace cannot be achieved at the boundary position of the desired translation workspace. The designed parameters are: L_1=96, L_3=92.2, R_0=156, and GCI=0.197. Fig. 11(b) shows that even though the minimum tilt angle of the real projected OW at the boundary position of Ω_{30} in the case of (b) ($\varpi_1 = 1, w_2 = 1, \varpi_3 = 0$) satisfies the desired minimum tilt angle (over 45°), the workspace shape becomes relatively irregular as a result of a low GCI value. The designed parameters are: L_1=84.6, L_3=105.8, R_0=42.7, and GCI=0.033. On the other hand, Fig.11 (c) shows that the projected OW in the case of (c) ($\varpi_1 = 1, w_2 = 1, \varpi_3 = 1$) can satisfy the desired minimum tilt angle and has a relatively regular workspace shape with a higher GCI value. The designed parameters are: L_1=96, L_3=99.1, R_0 =100.8, and GCI=0.120. In the case of (c), Fig. 12 shows that the size of the projected OW at the neutral position is larger than at the inside position or at the boundary position of the desired TW.

Table 5. Parameters optimized by genetic algorithm.

Type	r (mm)	$\theta_{\min}$ (°)	W_b	P_z (mm)	L_1 (mm)	L_3 (mm)	R_0 (mm)
Base				120	40	80	65
Optimized	30	45	1.5	195.1	96	99.1	100.8

Table 6. Performance indices for optimized parameters with $\theta_{\min}$ = 45° & $r = 30$ (mm).

Type	Ω				Γ				GCI
					P		B_k		At Ω_{30}
	± X (mm)	± Y (mm)	+Z (mm)	-Z (mm)	$\Gamma_{\max}$ (°)	$\Gamma_{\min}$ (°)	$\Gamma_{\max}$ (°)	$\Gamma_{\min}$ (°)	
Base	75	80	40	47	50	39	17	13	0.066
Optimized	93	107	96	107	69	62	51	45	0.120

Based on the optimum results of the suggested scheme, the following conclusions can be obtained: (1) the desired orientation workspace at the boundary positions of the desired translation workspace can be guaranteed with the specified $\theta_{\min}$, (2) the GCI value decreases with the increase in the desired translation and orientation workspaces, and vice versa, (3) the shape of the projected orientation workspace becomes more irregular as the GCI value becomes smaller, (4) if a desired TW and OW and GCI cannot be achieved by optimization, they can be achieved by increasing the constraints range of the design variables, as discussed in Section 4.3, which will also increase the size of a mechanism. Table 4 shows the performance tendency of the designed mechanism for the translational workspace (TW), the orientation workspace (OW), the global conditioning index (GCI), and the neutral height (P_z) with

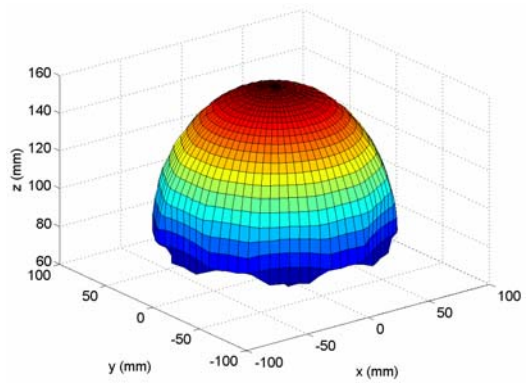

(a)

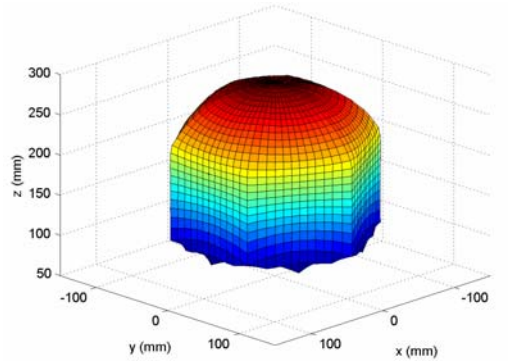

(b)

Fig. 13. Comparison of translational workspaces at each neutral position of end-effector: (a) **P** (0, 0, 120), (b) **P** (0, 0, 191.5) in Σ_b.

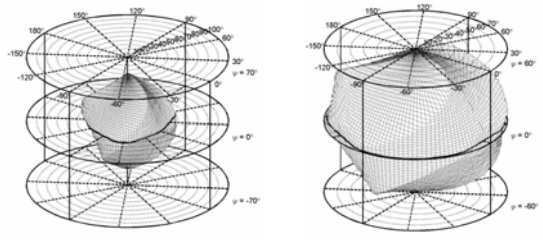

(a) Base model (b) Proposed model

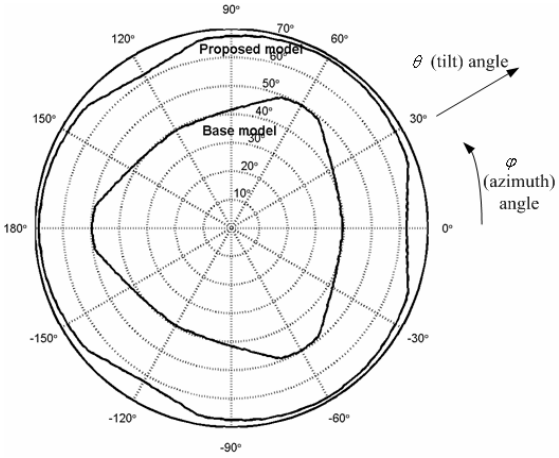

(c) Base/proposed models

Fig. 14. Comparison of rotational workspaces in cylindrical coordinates and projected rotational workspaces at each neutral position: (a) **P** (0, 0, 120), (b) **P** (0, 0, 191.5).

respect to the design variables L_1, L_3, and R_0 values.

5.2 Kinematic performance comparisons

In a comparison of the performance results before and after the optimization, the values chosen for the parameters L_1, L_3, and R_0 along with the values P_z are shown in Table 5 (see Fig. 1 for the optimized model and the manufactured device).

Table 6 lists the performance indices for the base and the proposed optimized models. To compare the relative isotropy for each case, the GCI was evaluated for Ω_{30}. Γ_x is defined as the tilt angle for the projected OW, where the subscript indicates the maximum tilt angle. In that case, $\Gamma_{\max}$ and $\Gamma_{\min}$ represent the minimum and maximum tilt values, respectively. Fig. 13 shows the volumes of the translation workspaces between the base and the proposed models. The size of a real translation workspace was determined at each neutral position **P** (0, 0, P_z) of the end-effector. The ranges of the three translational directions were ±75, ±80, 40, and –47 mm for the base model and ±93, ±107, 96, and –107 mm for the proposed model along the ±*X*, ±*Y*, *Z*, and –*Z* axes, respectively, in Σ_b. To compare the difference between the volumes, the workspace ratio for each axis *X*, *Y*, and *Z*, denoted by **v**, were 24, 34, and 133% where, for example, $v_Z = [|\pm Z|_{(b)} - |\pm Z|_{(a)})/|\pm Z|_{(a)}] \times 100\%$. Here, the subscripts *a* and *b* represent the smaller and larger of the two workspaces, respectively, and *Z* represents the corresponding axis for the workspace. The proposed model was much better than the base model with respect to the Z axis direction, which makes the shape of the translation workspace closer to spherical.

Fig. 14 shows the base and proposed orientation workspaces in cylindrical coordinates at each neutral position **P** of the end-effector. The ranges of the projected orientation workspaces were $39^\circ \le \Gamma_B \le 50^\circ$ and $62^\circ \le \Gamma_P \le 69^\circ$, where Γ_B and Γ_P are the tilt angles of the base and proposed models, respectively. The workspace ratio was e = 59%, where $v = \{ [(\Gamma_{P,\min} - \Gamma_{B,\min})]/ (\Gamma_{B,\min})\} \times 100\%$. Fig. 15 shows the base and proposed orientation workspaces at each **B** in Σ_o: each range was $13^\circ \le \Gamma_B \le 17^\circ$ and $45^\circ \le \Gamma_P \le 51^\circ$, and the workspace ratio was v = 246%. The orientation workspace volume on the boundary of the translational workspace in the proposed model was much larger than that of the base model. The GCI of the optimized model was 82% larger than the GCI of the base model.

Consequently, according to the GCI and the range of the translational and rotational motions, all of the kinematic performance indices of the proposed model were much better than those of the base model, even though it was about 63% larger in size. However, it should be noted that even though the base model was half the size of the original haptic device [12], the final size of the optimized mechanism was only 80% larger than the original device, given the three-times-increased OW. Since a haptic device, in order to perform its sophisticated work, requires both desired translation and orientation

Table 7. Workspace and size comparisons for different haptic devices.

Type	TW		OW (°)	Height (mm)	Width (mm)
	X (mm)	Z (mm)			
Suggested	200	200	69	195	230
Delta	360	300	20	600	700
Omni	160	70		200	203

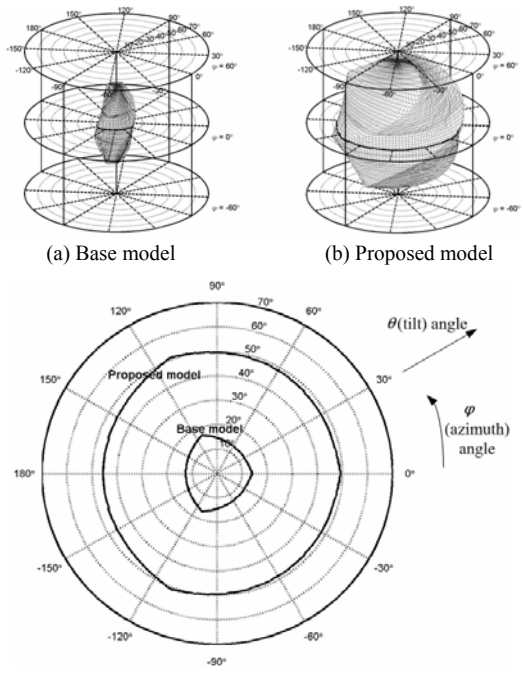

Fig. 15. Comparison of rotational workspaces in cylindrical coordinates and projected rotational workspaces at each boundary position **B** (-9.3, 0, 28.5) translated from neutral position.

workspaces and good isotropic characteristics, the proposed model is more efficient than the base model in terms of satisfying both workspaces and having more regular workspace shapes with a larger GCI.

6. Conclusions

When designing mechanisms for haptic devices, one should take into account the translation and orientation workspaces required for the various tasks, the isotropy required for the quality of the work, the singularities of the mechanism to provide easy control, and the compactness of the mechanism for effective utilization. Since these design variables have reciprocal relationships with each other, it is important to combine and manipulate them. Principally, parallel manipulators suffer from small workspaces, in particular the orientation workspace. This makes the application of parallel manipulators to haptic devices problematic. From this point of a view, we presented an optimal design scheme for a six-DOF parallel manipulator that required both 3-D translation and orientation workspaces as well as isotropy for a haptic device application. In the optimization process, an objective function was designed for three kinematic performance indices: the translation workspace, the orientation workspace at the boundary positions of the desired translation workspace, and the GCI. The function was maximized using a genetic algorithm, and the optimal performance indices were synthesized together to obtain the design linkage parameters. By discretizing a translation workspace with a desired spherical surface at a neutral position and by discretizing a projected orientation workspace with a desired minimum tilt angle with respect to the azimuth angle at each boundary position of the desired discrete translation workspace, the optimized mechanism was made to satisfy the specified orientation workspace, even at the boundary surface of the desired translational workspace. Therefore, the proposed haptic device with an optimized parallel manipulator guaranteed the required orientation workspace throughout the prescribed 3-D translational workspace. The relative size of the device could be determined from the *Z* coordinate of its neutral position, which could be calculated from the optimized design parameters. The performances of all of the kinematic parameters of the optimized model were improved compared with those of the existing base model, except for the size. After optimization, the projected orientation workspace was increased by about 60% at its neutral position, and about threefold at its translated position, compared with the projected OW of the base model. The translation workspace of the *Z* axis was 140% larger in the proposed model and was closer to a spherical shape, and had an 80%-increased GCI. It should be noted that, as shown in Table 7, the real translation workspace (186mm (x axis), 214mm (y axis), 203mm (z axis)) for the designed mechanism is larger than that (160mm (x axis), 120mm (y axis), 70 mm (z axis)) of the PHANTOM® Omni™, though the difference is slight. The workspaces and sizes of the commercialized 6-DOF Delta Haptic Device with parallel structures from Force Dimension Corporation are comparable to those of the suggested device. The suggested device achieved an especially large orientation workspace compared with that of the DELTA device. (Other kinematic comparisons among similar parallel manipulators had been performed in a previous paper [12].) The proposed haptic device based on this optimized mechanism, therefore, will allow a user to safely perform virtual assembly tasks with both translational and rotational motions within the specified workspaces. In future work, dynamic parameters for mechanism optimization, such as inertia, mass, and friction will be considered.

Acknowledgements

This work was by Priority Research Centers Program through the National Research Foundation of Korea (NRF) funded by the Ministry of Education, Science and Technology (2009-0094016) and supported by the Ministry of Knowledge Economy (MKE), Korea, under the Information Technology Research Center support program supervised by the National

IT Industry Promotion Agency (NIPA; NIPA-2010-C1090 - 1031- 0006).

Nomenclature

$\Sigma_b (X_b, Y_b, Z_b)$	:	Global reference frame
$\Sigma_{o'} (X_{o'}, Y_{o'}, Z_{o'})$	:	Local frames of end-effector
$\Sigma_{pi} (X_{pi}, Y_{pi}, Z_{pi})$	:	Local frames of each pantograph
R_0 and R_1	:	Radius of base and end-effector, respectively
δ_i	:	Axisymmetric positions of each pantograph with radii of R_0
γ_i	:	Axisymmetric positions of each pantograph and revolute joint with radii of R_1
SL	:	Offset distance between original centers and actual centers of spherical joints
L_1	:	Upper links of pantograph
L_2	:	Lower links of pantograph
L_3	:	Connecting bars
M_i	:	Positions of active joints
Q_i	:	Positions of revolute joints
E_i	:	Positions of revolute joints
θ_{1i} and θ_{2i}	:	Active joint angles of each pantograph
$x, y, z, \varphi, \theta, \gamma$	:	Given position and rotation of end-effector
$\mathbf{P}$ $(0, 0, P_z)$	:	Neutral position of end-effector along Z axis in Σ_b
Ω_r	:	Sphere whose center is located at $\mathbf{P}$ $(0, 0, P_z)$ in Σ_b, where subscript indicates desired radius of sphere
$\mathbf{B}_k (X_k, Y_k, Z_k)$	:	Discrete translation points
$\Gamma(\theta_{\min})$	:	Projected orientation workspace (OW), where subscript $\theta_{\min}$ indicates desired minimum tilt angle
Γ_x	:	Tilt angle for projected OW
$\sigma_{\max}$ and $\sigma_{\min}$	:	Maximum and minimum singular values of manipulator Jacobian $\mathbf{J}$
c	:	Condition number
η	:	Index that is inversely proportional to condition number
CL	:	Characteristic length for geometric interpretation
R	:	Radius of operation sphere
n_{in}	:	Number of discretized points that fall in desired translation workspace Ω_r with respect to discrete point $\mathbf{B}_i (X_i, Y_i, Z_i)$
$M_{i,\,in}$	:	Number of discretized angles that fall in desired projected OW $\Gamma(\theta_{\min})$ with respect to discrete point $\mathbf{B}_i (X_i, Y_i, Z_i)$
$\varpi_1, \varpi_2, \varpi_3$	:	Weighting factors for optimization
N_{tot} and M_{tot}	:	Total number of discretized points and angles, respectively
N	:	Integer for total discretized number $N_{\text{tot}}=N(N-1)+2$
Λ	:	Design variable constraints for system boundary
$\boldsymbol{x}^{(L)}$ and $\boldsymbol{x}^{(U)}$	:	Lower and upper limiting vector for $\boldsymbol{x} = (L_1, L_3, R_0)$, respectively
$\boldsymbol{x}_{init}$	:	Initial design vector value
W_b	:	Constraint range gain
v	:	Workspace ratio for each axis
$\boldsymbol{s}$	:	Vector of binary string
$\boldsymbol{l}$	:	Vector of chromosome length
$P_a(k)$	:	Population in k-th generation
N_P	:	Population size
P_c	:	Probability of crossover
P_m	:	Probability of mutation

References

[1] L. J. Stocco, S. E. Salcudean and F. Sassani, Optimal kinematic design of a haptic pen, *IEEE/ASME Transactions on Mechatronics,* 6 (3) (2001) 210-220.

[2] X. Kong and C. Gosselin, Kinematics and singularity analysis of a novel type of 3- CRR 3-DOF translational parallel manipulator, *The International Journal of Robotics Research,* 21 (9) (2002) 791-798.

[3] K. Vlachos and E. Papadopoulos, Design and implementation of a haptic device for training in urological operations, *IEEE Transactions on Robotics and Automation,* 19 (5) (2003) 801-809.

[4] J. Merlet, C. Gosselin and N. Mouly, Workspaces of planar parallel manipulator, *Mechanism and Machine Theory,* 33 (1/2) (1998) 7-20.

[5] F. Bulca, J. Angeles and P. J. Zsombor-Murray, On the workspace determination of spherical serial and platform mechanisms, *Mechanism and Machine Theory,* 34 (1999) 497-512.

[6] A. Kosinska, M. Galicki and K. Kedzior, Designing and optimization of parameters of delta-4 parallel manipulator for a given workspace, *Journal of Robotic Systems,* 20 (9) (2003) 539-548.

[7] M. Arsenault and R. Boudreau, The synthesis of three-degrees-of-freedom planar parallel mechanisms with revolute joints (3-RRR) for an optimal singularity-free workspace, *Journal of Robotic Systems,* 21 (5) (2004) 259-274.

[8] K. Y. Tsai and K. D. Huang, The design of isotropic 6-DOF parallel manipulators using isotropy generators, *Mechanism and Machine Theory,* (38) (2003) 1199-1214.

[9] K. Y. Tsai and S. R. Zhou, The optimum design of 6-DOF isotropic parallel manipulators, *Journal of Robotic Systems,* 22 (6) (2005) 333-340.

[10] M. Gallant and R. Boudreau, The synthesis of planar parallel manipulators with prismatic joints for an optimal, singularity-free workspace, *Journal of Robotic Systems,* 19 (1) (2002) 13-24.

[11] B. Monsarrat and C. M. Gosselin, Workspace analysis and optimal design of a 3-leg 6-dOF parallel platform mechanism, *IEEE Transactions on Robotics and Automation,* 19

(6) (2003) 954-966.
[12] J. Yoon and J. Ryu, Design, fabrication, and evaluation of a new haptic device using a parallel mechanism, *IEEE/ASME Transactions on Mechatronics,* 6 (3) (2001) 221-233.
[13] Y.-K. Hwang, Jung-Won Yoon, Christiand, and Je-Ha Ryu, "The Optimum Design of a 6-DOF Parallel Manipulator with Large Orientation Workspace", *IEEE International Conference on Robotics and Automation 2007 (ICRA 2007)*, Rome, Italia, Rome, (2007).
[14] I. A. Bonev, J. Ryu, A new approach to orientation workspace analysis of 6-DOF parallel manipulators, *Mechanism and Machine Theory,* 36 (2001) 15-28.
[15] C. Gosselin, J. Angeles, A global performance index for the kinematic optimization of robotic manipulator, *Transactions of the ASME Journal of Mechanical Design,* 113 (1991) 220-2261.
[16] M. Tandirci, J. Angeles and F. Ranjbaran, The characteristic point and characteristic length of robotic manipulators, *Proc. ASME 22nd Biennial Conf. Robotics, Spatial Mechanics, Mechanical Systems*, vol. 45, Scottsdale, AZ, (1992) 203-208.
[17] S. Kim and J. Ryu, New dimensionally-homogeneous Jacobian matrix formulation by three end-effector points for optimal design of parallel manipulators, *IEEE Transactions on Robotics and Automation*, 19 (4) (2003) 731-737.
[18] G. Nawratil, New performance indices for 6R robots, *Mechanism and Machine Theory,* 36 (2001) 15-28.
[19] J. H. Holland, *Adaptation in natural and artificial systems*, The University of Michigan Press, Michigan, USA, (1975).
[20] M. Mitchell, *An introduction to genetic algorithm*, The MIT press, Cambridge, MA, USA, (1998).
[21] Christiand, J. Yoon and P. Kumar, A Novel Optimal Assembly Algorithm for Haptic Interface Applications of a Virtual Maintenance System, *Journal of Mechanical Science and Technology,* 23 (1) (2009) 183-194.

Jungwon Yoon received the Ph.D in the Department of Mechatronics in 2005 from Gwangju Institute of Science and Technology (GIST). He had worked as a senior researcher in Electronics Telecommunication Research Institute (ETRI), Daejeon, Korea, and a visiting researcher at Virtual Reality Lab, the Rutgers University, U.S.A, from 2001 to 2002. In 2005, he joined the School of Mechanical & Aerospace Engineering, Gyeongsang National University, Jinju, Korea, where he is currently an assistant professor. In 2010-2011, he also joined the Center for Neuroscience and Regenerative Medicine, National Institutes of Health as Visiting Fellow. His research interests include virtual reality haptic devices & locomotion interfaces, and rehabilitation robots.

Jeha Ryu is a professor of the Mechatronics Department at the Gwangju Institute of Science and Technology (GIST). He is the director of national Haptics Technology Research Center. His research interests include haptics, haptic rendering, haptic interaction control, design and control of haptic devices, as well as haptic-included modeling and broadcasting. Ryu received a PhD degree in Mechanical Engineering from the University of Iowa, USA.